Analyst

ROYAL SOCIETY OF CHEMISTRY

PAPER

View Article Online
View Journal

Cite this: DOI: 10.1039/d0an00470g

An electrochemical biosensor based on methylene blue-loaded nanocomposites as signal-amplifying tags to detect pathogenic bacteria

Shengjun Bu,[a] Kuiyu Wang,[a,b] Zhongyi Li,[a] Chengyu Wang,[a] Zhuo Hao,[a] Wensen Liu*[a] and Jiayu Wan *[a]

Received 8th March 2020,
Accepted 26th April 2020

DOI: 10.1039/d0an00470g

rsc.li/analyst

A sandwich-type electrochemical biosensor was successfully constructed for the sensitive detection of pathogenic bacteria. In this biosensor platform, methylene blue (MB) organic–inorganic nanocomposites (MB@MI) were synthesized from magainin I (MI, antimicrobial peptide specific to *Escherichia coli* O157:H7), $Cu_3(PO_4)_2$ and MB *via* a one-pot method, and were explored as a novel electrochemical signal label of biosensors generating amplified electrochemical signals by differential pulse voltammetry (DPV). *E. coli* O157:H7 specifically sandwich bound to the aptamers on the electrode surface and MB@MI nanocomposites, and the changes in the current signal generated on the electrode surface were used for the quantitative determination of *E. coli* O157:H7. Under optimum conditions, the proposed biosensor showed excellent performance with a wide linear range of 10^2–10^7 CFU mL^{-1} and a low detection limit of 32 CFU mL^{-1}, featuring favorable selectivity, repeatability and stability. According to the experiments conducted on real samples, the proposed approach is capable of detecting pathogenic bacteria in clinical diagnostics.

Introduction

Food-borne diseases caused by contamination with pathogenic bacteria pose a major threat to public health and have become a global food safety issue. Rapid and accurate assay of pathogenic bacteria in food is important for the prevention and control of food-borne diseases.[1] Currently, the detection of food-borne pathogenic bacteria in food still relies on conventional culture methods, considered as the gold standard, but their disadvantage is the long testing cycle. Enzyme-linked immunosorbent assay (ELISA),[2] polymerase chain reaction (PCR),[3] DNA probes,[4] gene chip techniques[5] and other modern detection methods are also used for the detection of pathogenic bacteria in food.[6] Although these methods have good specificity and high sensitivity, they are time consuming, laborious, impractical and, more importantly, not suitable for field and real-time applications.

Various biosensors have been developed for the detection of pathogenic bacteria, such as electrochemical,[7] optical,[8] and fluorescence[9] sensors. Compared with other approaches, electrochemical biosensors have attracted particular attention due to their ease of miniaturization, simplicity, rapid responsiveness, sensitivity and low cost.[10] A new electrochemical signal label must be introduced to construct a novel sandwich-type electrochemical immunosensor for detecting pathogenic bacteria. Methylene blue (MB), a mediator of electron transfer, is responsible for electron production and signal amplification in an electrochemical biosensor, and it has wide applications in sensing.[11] MB can be used to form electrochemically functional nanocomposites on nanomaterial surfaces as a signal label of electrochemical immunosensors. Some nanomaterials (*e.g.* UiO-66 metal–organic framework[12] and AuPt bimetallic nanoparticles[11]) have been used as support materials to immobilize MB, and the synthesized MB nanocomposites are used as signal labels for fabricating dual-signal sandwich electrochemical immunosensors.

The development of novel nanocomposites for electrochemical immunosensors has aroused widespread interest. Inspired by natural biomineralization, all kinds of biomacromolecules, such as proteins,[13] polysaccharides,[14] and nucleic acids,[15] have been used as biomolecular templates for biological mineralization, thus obtaining organic–inorganic hybrid materials with controllable morphology and excellent properties.[16] The flower-like organic–inorganic hybrid nanocomposites are prepared through an eco-friendly one-pot strategy. The activity and stability of biomolecules immobilized in

[a]*Institute of Military Veterinary, Academy of Military Medical Sciences, Changchun, 130122, China. E-mail: Liuws85952@163.com, wanjiayu@hotmail.com; Fax: +86 86985828; Tel: +86 86985951*
[b]*Southern Laboratory of Ocean Science and Engineering, School of Chemical Engineering and Technology, Sun Yat-sen University, Guangdong, 519082, China*

organic–inorganic nanocomplexes have been significantly enhanced, and the synthesized nanocomplexes have been widely used in immunological analysis.[17]

The three-dimensional shape of flower-like, organic–inorganic hybrid nanocomposites, especially the application of nanomaterial immobilization, has attracted widespread attention.[18] The flower-like nanocomposites with large surface areas can provide more active sites to guarantee the loading of more nanomaterials, and nanomaterials can be adsorbed into the gaps of petals, maintaining the stability of nanomaterials.[19] Therefore, the flower-like nanocomposites as nanomaterial carriers have broad application prospects in the biosensing field.[20] Wan's group observed that the flower-like nanocomposites could load a large number of nanoparticles (hemin, platinum, *etc.*), generating and amplifying signals in biosensors.[21,22]

To promote the utilization of MB as the signal label of electrochemical immunosensors for sensitive target detection, flower-like organic–inorganic nanocomposites loaded with MB were synthesized. In this work, an electrochemical biosensor was designed for the rapid detection of pathogenic bacteria (Scheme 1). For the ultrasensitive detection of *Escherichia coli* O157:H7, hybrid nanocomposites loaded with MB were introduced as signal labels to fabricate a novel, sandwich-type electrochemical biosensor. The flower-like nanocomposites were prepared from MI (antimicrobial peptide specific to *E. coli* O157:H7), $Cu_3(PO_4)_2$ and MB *via* a one-pot method, and MB was loaded on the antimicrobial peptide–$Cu_3(PO_4)_2$ nanocomposites. MI is a new kind of bio-recognition antimicrobial peptide that has recently been used in the rapid and sensitive detection of pathogenic bacteria, and it has attracted increasing attention because of its outstanding superiority in the testing field.[23] Under severe environmental conditions, such as thermal (boiling/autoclaving) and chemical denaturation, MI has greater stability than typical spherical proteins and it could maintain its activity against pathogenic bacteria.[24,25] The thiol-modified aptamers of *E. coli* O157:H7 have been explored for modification on the electrode surface by Au–S binding. Aptamers, single-stranded RNA or DNA oligonucleotides, can efficiently and specifically bind to several pathogenic bacteria. Compared with antibodies, aptamers have some advantages, including simple and rapid synthesis, high affinity, good stability, flexible modification, resistance to denaturation, and low cost.[26] Aptamer-based electrochemical immunoassays have been reported for the detection of pathogenic bacteria as they can overcome many limitations of antibodies.[27] As a result, a sandwich electrochemical biosensor was fabricated, which could achieve point-of-care and sensitive detection of pathogenic bacteria. The novelty of this paper was to synthesize MB@MI organic–inorganic nanocomposites as electrochemical signal labels of the proposed biosensor. This biosensor may satisfy the requirements for point-of-care clinical diagnosis, which provides a versatile strategy and new avenue for the diagnosis of pathogenic bacteria.

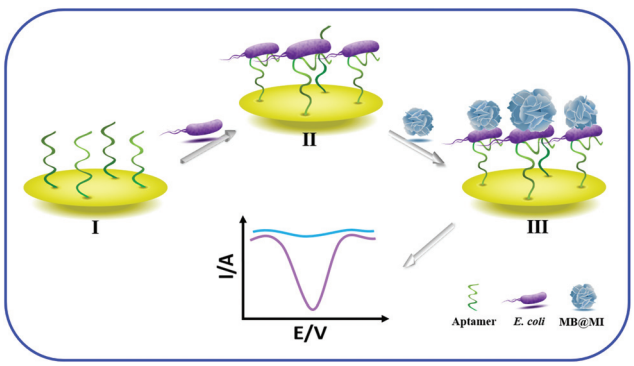

Scheme 1 Schematic diagram of the amplified sandwich-type immunosensor strategy for the detection of pathogenic bacteria based on MB@MI. (I) Modification of the gold electrode. (II) Process of aptamer recognition of the target. (III) Process of signal tag (MB@MI) output.

Methods and materials

Materials and reagents

The aptamer of *E. coli* O157:H7 (5′-ATACGGGAGCCAACACC-ATAATATGC CGTAAGGAGAGGCCTGTTGGGAGCGCCGTAGAG-CAGGTGTGACGGATTTTTTTTT-3′) with thiol modification at the 3′ end was selected, as described previously,[28] and purified by reversed-phase HPLC. 6-Mercapto-1-hexanol (MCH) and tris (2-carboxyethyl)phosphine hydrochloride (TCEP) were purchased from Sigma-Aldrich (St Louis, MO, USA). $CuSO_4{\cdot}5H_2O$, PBS (consisting of 0.01 M NaH_2PO_4 and 0.01 M Na_2HPO_4, pH 7.4), MB, and magainin I (MI: GIGKFLHSAGKFGKAFVGEIMKS) were purchased from Sangon Biotechnology Co. Ltd (Shanghai, China). The storage buffer used for oligonucleotides was 10 mM pH 8.0 tris(hydroxymethyl)aminomethane (Tris-HCl) containing 1 mM EDTA. The aptamer was dissolved in 10 mM Tris-HCl stock solution (pH 7.4, 50 mM NaCl) at 4 °C until use. Tris-HCl buffer containing 10 mM Tris and 50 mM NaCl was used as a reaction buffer (pH 7.4). The washing buffer (pH 7.4) contained 20 mM Tris, 0.1 M NaCl, 5.0 mM $MgCl_2$ and 0.05% Tween-20. All other participating reagents were of analytical reagent grade and used untreated as purchased, and various buffer solutions were prepared with ultrapure water treated using a Milli-Q water purification system (≥18 MΩ; Bedford, MA, USA) and used in all experiments. *E. coli* O157:H7, *S. aureus* and *S. typhimurium* were all used in a concentration of 10^7 CFU mL^{-1} in 0.1 mM PBS.

E. coli O157:H7 CICC 10899, *Staphylococcus aureus* CICC 10145, *Listeria monocytogenes* CICC 21529 and *Salmonella typhimurium* CICC 21484 strains were obtained from the China Center of Industrial Culture Collection (CICC).

Apparatus

Scanning electron microscopy (SEM) images were obtained using a JEOL JSM7900F microscope (Beijing, China). Electrochemical measurements including differential pulse voltammetry (DPV) and cyclic voltammetry (CV) were carried out on a CHI 660E electrochemical workstation (Shanghai

Chenhua Instruments Co. Ltd, China). Electrochemical detection was performed on a conventional three-electrode system containing a gold electrode as the working area with 2 mm diameter (area = 0.03 cm^2), a platinum wire as the auxiliary electrode, and Ag/AgCl (3 M KCl) as the reference electrode. All electrodes were purchased from Shanghai Chenhua Instruments Co. Ltd. Cyclic voltammograms (CVs) were recorded at a scan rate of 100 mV s^{-1} and in the potential range between −0.2 and 0.6 V. DPV measurement was performed in 10 mM Tris-HCl solution (pH 7.4) containing 50 mM NaCl in the potential range from −0.1 to −0.70 V at a pulse amplitude of 10 mV. Powder X-ray diffraction (XRD) patterns were measured using an XD6 X-ray diffractometer (Beijing, China) with Cu Kα radiation. All the experiments were carried out at room temperature (25 °C).

Pretreatment of the aptamer

Before use, the aptamer targets were prepared as described previously,[29] with slight modifications. The aptamer was denatured by heating at 90 °C for 5 min, and quickly refluxed for 15 min at 4 °C. Finally, it was allowed to stand at room temperature for 8 min to renature the aptamer before immobilization on the electrode, to attain its most stable conformation for successful binding to its target.

Bacteria preparation

E. coli O157:H7 and other food pathogenic bacteria used in this assay were grown in Luria–Bertani broth at 37 °C by shaking in an incubator for 12 h. The bacterial concentrations were estimated and recorded by measuring the optical density at 600 nm. Bacterial cultures were centrifuged at 6000 rpm for 10 min and washed with 0.1 mM PBS (pH 7.4). Serial concentrations (10–10^8 CFU mL^{-1}) of the target bacteria were prepared by diluting the original solution with 0.1 mM PBS and storing at 4 °C.

Preparation of MB@MI nanocomposites

The MB@MI nanocomposites were prepared according to the previous report[30] with a slight modification. MB (10 μM) and MI (5 μg mL^{-1}) were dispersed in 1 mL of PBS (pH 7.4, 10 mM) containing 20 μL of $CuSO_4{\cdot}5H_2O$ (120 mM) aqueous solution and stirred to attain the final mixture. The mixture was reacted to form MB@MI nanocomposites overnight at room temperature. Finally, the solution was centrifuged (8000 rpm) and washed in 0.1 mM PBS three times and stored at 4 °C when not used. This mixture (Cu^{2+}, MI and MB molecules) served as nucleation sites for the primary crystals of copper phosphate at the early growth stage. Then the nanoparticles were grown by interactions between these proteins, organics and Cu^{2+}, and eventually MB@MI nanocomposites were formed. The pure MB@MI nanocomposites obtained with this procedure had high conductivity (MB has electron conductivity) and high specific surface area with a large population of MI that lead to better recognition and transduction of targets. The structure of the MB@MI nanocomposites was determined by SEM.

Pretreatment and surface modification of the gold electrode and the *E. coli* O157:H7 detection procedure

A bare gold electrode (2 mm in diameter) was polished using 1.0 μm, 0.3 μm and 0.05 μm alumina powder to a mirror-like finish, followed by thorough rinsing by sonication in ethanol and deionized water for 5 min. The polished gold electrode was immersed in a fresh Piranha solution (30% H_2O_2 : 98% H_2SO_4 = 1 : 3 v/v) and 50% nitric acid for 10 min and 30 min, respectively, followed by ultrasonication in deionized water to remove contaminants on the electrode surface, and then dried under nitrogen. After this, the working electrode was electrochemically activated in 0.5 M H_2SO_4 by potential scanning between 0.2 and 1.0 V, with a scan rate of 50 mV s^{-1}, until a reproducible CV was obtained.

To modify the gold electrode, it was incubated overnight with a 2 μM aptamer (AP) probe (dissolved in 10 mM Tris-HCl with 1 mM TCEP for 30 min to break the disulfide bond before use) at 25 °C to form an aptamer layer on the surface, and then rinsed thoroughly with washing buffer. To block the non-specific sites at the surface of the electrode, 1 mM MCH (aqueous solution) was incubated with the aptamer-modified gold electrode for 1 h at room temperature. For detection, different concentrations of *E. coli* O157:H7 (dissolved in 1 mM PBS) were added dropwise onto the modified electrode surface (AP/MCH/Au electrode) at 25 °C for 2 h. Next, the electrode was soaked in MB@MI for 30 min at 25 °C to achieve the sandwich structure. After each modification step, the electrode immunosensor was washed thoroughly with washing buffer. By independent experiments, each step was repeatedly performed no less than three times.

Results and discussion

Characterization of nanocomposites and electrochemical feasibility of the design principle

Inspired by the biomineralization process, the antimicrobial peptide MI and MB were simply mixed into the PBS solution (Cu^{2+}) to prepare MB@MI at room temperature. The approach was simple and did not require toxic elements or complicated purification processes. SEM was used to analyse the morphology of the nanocomposites (Fig. 1a and b). MB@MI was found to have uniform hierarchical structures with flower-like nanostructures with an average diameter of ~2.5 μm. The substrate recognition ability and biocatalytic activity of MB@MI were improved by increasing the specific surface area, the layer-by-layer polymeric nanostructure of MB@MI could encapsulate the amounts of MB and MI. The crystal structure of the synthesized MB@MI was characterized by XRD (Fig. 1c). The main diffraction peaks of MB@MI were at 7.38°, 12.84°, 29.5° and 33.78°, which agreed with those of $Cu_3(PO_4)_2$ (JCPDS: 22-0548). For the verification of the feasibility of the design principle, we conducted experiments with and without the target *E. coli* O157:H7 sensor on the electrode to compare the DPV responses. No redox peaks (black curve) could be observed without the target in the gold electrode (Fig. 1d). After modifi-

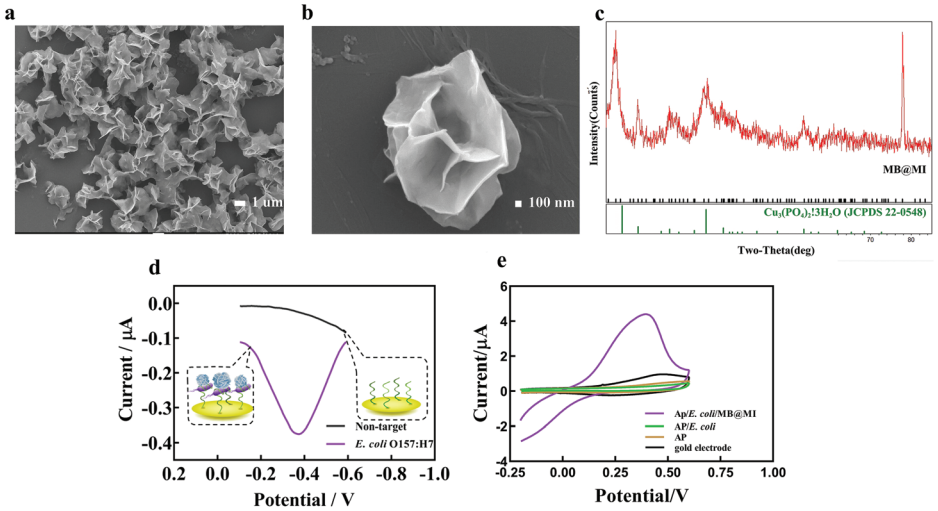

Fig. 1 SEM images of MB@MI at a scale of 1 μm (a) and 100 nm (b). The average size of MB@MI was ~3 μm. (c) XRD of MB@MI showing peaks for $Cu_3(PO_4)_2{\cdot}3H_2O$ (JCPDS 22-0548). DPV (d) and CV (e) signals of the prepared electrochemical immunosensor after sensing with or without *E. coli* O157:H7 (10^7 CFU mL^{-1}) in 100 mM PBS containing 1.0 mM NaCl.

cation with the target and signal tag, the redox peak current (purple curve) increased significantly because MB@MI nanocomposites successfully formed sandwich structures with the targets and aptamer probes on the gold electrode. As shown in Fig. 1e, after the modification of the electrode with AP and *E. coli* O157:H7, the CV current was reduced because AP and the target bacteria can slightly hinder the electron transfer. However, the peak currents of the electrode increased distinctly after coupling of the MB@MI nanocomposites, indicating a rapid electron transfer. The DPV and CV responses of the immunosensor based on the synthesized sensor of MB@MI were successfully immobilized on the gold disk electrodes.

Optimization of the experimental conditions

To achieve high detection sensitivity, assay parameters, such as the concentration of the captured aptamers, concentration of signal probe nanocomposites, incubation temperature, and incubation time, were optimized. The target bacteria at a concentration of 10^5 CFU mL^{-1} were used to optimize the parameters. The captured aptamers fixed on the gold electrode surface affected the electrochemical response of the immunosensor. As the captured probe, the concentration of aptamers ranged from 0.5 to 2.0 μM. Theoretically, the more the captured aptamer was fixed, the greater the electrochemical signal was observed. However, too many captured aptamers immobilized on the Au electrode surface can hinder electron transfer on the surface of the electrode, reducing the sensitivity of the biosensor. The maximum current signal was obtained at 1.0 μM (Fig. 2A). The recognition efficiency between the signal probe and *E. coli* O157:H7, and current signal amplification were, respectively, influenced by the amount of MI and MB immobilized in the hybrid nanocomposites. In the preparation of hybrid nanocomposites, different concentrations of MB and MI were analyzed. The current signal increased with the concentration of MB, and it was maximum when the concentration of MB reached 10 μM; then the current signal began to decline with a further increase of the MB concentration (Fig. 2C). Therefore, 10 μM MB was chosen to prepare MB@MI. The current signal increased with the increase of the concentration of MI, and the current signal decreased when the concentration of MI reached 5 μg mL^{-1} (Fig. 2B). Therefore, 5 μg mL^{-1} MI was selected to prepare MB@MI. As the volume of MB@MI increased from 250 to 350 μL, the current responses were increased. When the concentration of the captured aptamers exceeded 350 μL, the current responses began to decrease. Therefore, 350 μL was the optimum volume of MB@MI for preparing immunosensors (Fig. 2D).

Incubation time and temperature had important effects on biosensor sensitivity. Different incubation times for *E. coli* O157:H7 from 60 to 180 min and MB@MI from 15 to 75 min were analyzed (Fig. 3). The optimal incubation times of 30 min for MB@MI and 120 min for *E. coli* O157:H7 were used in this study. The incubation temperature of 4–37 °C was used for the detection of the target bacteria. The current signal was maximum when the incubation temperature was 25 °C. Therefore, the optimal incubation temperature was selected as 25 °C.

Sensitivity of the proposed immunosensor

To examine the sensitivity of the proposed approach, various concentrations of *E. coli* O157:H7 under the optimal experimental conditions were further studied by DPV (Fig. 4). A decline in the DPV signal with some concentrations was recorded, which coincided with what we designed. Good linear dependence between the current changes and the logarithm of the concentrations of *E. coli* O157:H7 ranged from 10^2 to 10^7 CFU mL^{-1}, and the detection limit was 32 CFU mL^{-1}. The fitted linear regression equation is $Y = -0.04965 \times X + 0.04137$ ($R^2 = 0.9932$). The comparative analytical performance (detection range and limit) between the designed method and other

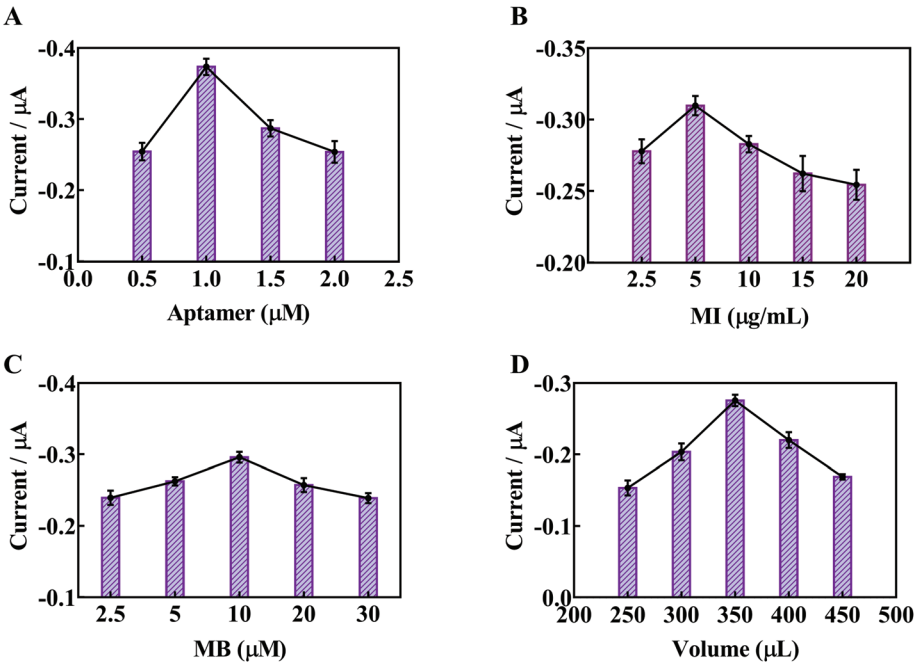

Fig. 2 Effect of (A) different concentrations of aptamers of 0.5, 1.0, 1.5 and 2.0 μM; (B) MB loading concentration of 2.5, 5, 10, 20 and 30 μM; (C) MI loading concentration of 2.5, 5, 10, 15 and 20 μM; and (D) nanocomposite volume of 250, 300, 350, 400 and 450 μL.

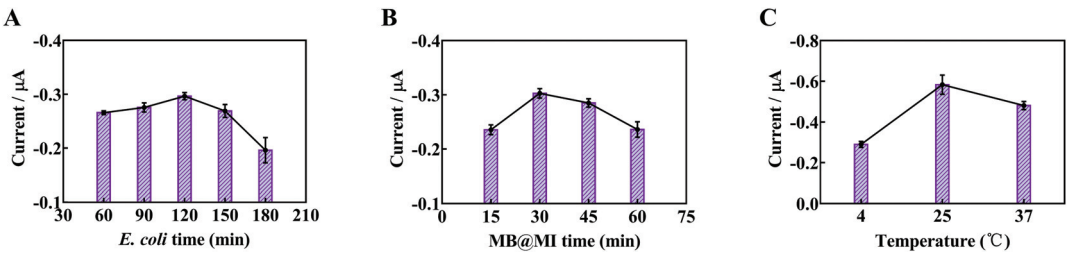

Fig. 3 Effect of (A) time of MB@MI nanocomposite incubation, (B) time of *E. coli* O157:H7 incubation, and (C) temperature of incubation.

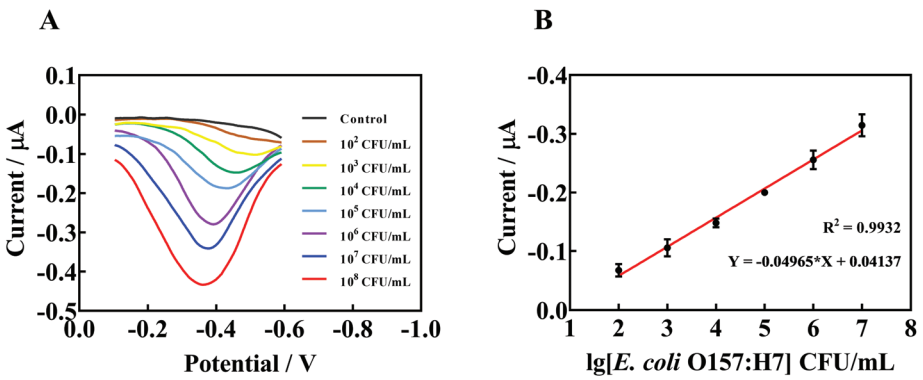

Fig. 4 (A) DPV responses of our designed biosensor toward different concentrations ranging from 10 to 10^8 CFU mL^{-1} for *E. coli* O157:H7. (B) The calibration plot between the current intensity of the logarithm of *E. coli* O157:H7 and the DPV peak current (the error bars are standard deviations for $n = 3$).

Table 1 Comparison of different electrochemical techniques for the detection of *E. coli* O157:H7

Analytical method	Target	Linear range (CFU mL^{-1})	Detection limit (CFU mL^{-1})	Ref.
EIS	*Bacillus anthracis*	10^4–5×10^6	3×10^3	29
DPV	*E. coli* O157:H7	2.1×10^1–2.1×10^7	21	31
EIS	*S. typhimurium*	10–10^8	10	32
LSV	*E. coli*	10^3–10^8	200	33
EIS	*Listeria* cells	1.6×10^2–1.6×10^5	160	34
EIS	*E. coli* O157:H7	10^2–10^6	290	35
DPV	*E. coli* O157:H7	10^2–10^7	32	Our work

EIS, electrochemical impedance spectroscopy; CA, chronoamperometry; LSV, linear sweep voltammetry.

reported detection methods is shown in Table 1. Compared to other approaches, the designed method achieved excellent performance for detecting *E. coli* O157:H7, with a LOD of 32 CFU mL^{-1}. The lower LOD of the approach may be attributed to more MB-loaded nanocomposites as signal-amplifying tags.

Specificity

To analyze the specificity of the approach, we chose three pathogenic bacteria: *S. typhimurium* (*Sal*), *S. aureus* (*Sta*) and *L. monocytogenes* (*Lis*) as the nontarget pathogenic bacteria. Compared with the blank experiment with non-target pathogenic bacteria, the current change in the designed method caused no significant signal change (Fig. 5). This was attributed to the specific recognition of the captured aptamer probe and the signal probe nanocomposites. The selected aptamers and antimicrobial peptides could specifically identify *E. coli* O157:H7. This guarantees the specificity of this method and resists the interference of other bacteria.[28] These results demonstrated that the designed approach for detecting *E. coli* O157:H7 (*E. coli*) had excellent specificity.

Real sample analysis

To verify the application and reliability of the electrochemical method for detecting pathogenic bacteria, the electrochemical immunosensor was used to detect *E. coli* O157:H7 based on the standard addition method. Various concentrations of *E. coli* O157:H7 (10^3, 10^4 and 10^5 CFU mL^{-1}) were spiked into pure milk (Table 2). The recovery of the detected *E. coli* O157:H7 *via* DPV was 88.1–115.3% and the variation of relative standard deviation (RSD) ranged from 0.7 to 3.9%. These results indicate that the MB@MI immunosensor has the capability to be used for the electrochemical detection of pathogenic bacteria in complex samples.

Table 2 Different concentrations of *E. coli* O157:H7 mixed in pure milk samples

Original value (CFU mL^{-1})	*E. coli* O157:H7 added (CFU mL^{-1})	*E. coli* O157:H7 found (mean ± RSD, CFU mL^{-1})	Recovery (%)
0	1×10^3	$(0.881 \pm 0.007) \times 10^3$	88.1 ± 0.7
0	1×10^4	$(0.992 \pm 0.034) \times 10^4$	99.2 ± 3.4
0	1×10^5	$(1.153 \pm 0.039) \times 10^5$	115.3 ± 3.9

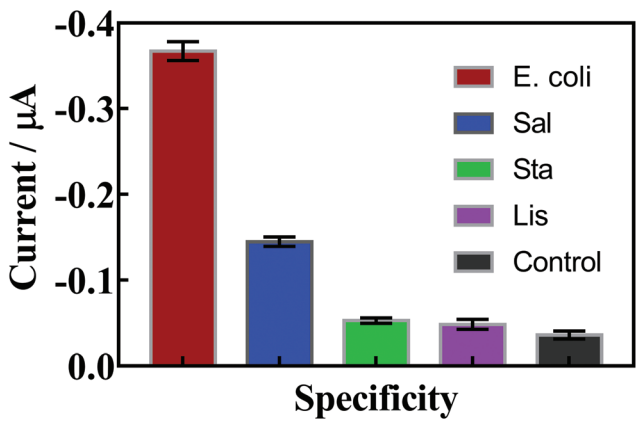

Fig. 5 Specificity of the electrochemical immunosensor for the detection of different targets. The concentration of all bacteria was 10^7 CFU mL^{-1}. 0.1 mM Tris buffer was used as a control.

Conclusions

A novel electrochemical biosensor was simply designed for highly sensitive and selective detection of pathogenic bacteria using the captured aptamer probes and MB-loaded nanocomposite-based signal tags. This approach has a distinct advantage, that is the nanocomposite MB@MI has excellent signal amplification without any extra modification because of its specific nanostructure. Therefore, under optimum conditions, the electrochemical biosensor detected *E. coli* O157:H7 at a concentration range of 10^2–10^7 CFU mL^{-1}, with a method detection limit of 32 CFU mL^{-1}. The immunosensor for *E. coli* O157:H7 detection showed high specificity, excellent reproducibility and acceptable stability. Thus, this low cost and highly sensitive and selective *E. coli* O157:H7 biosensor is explored as a promising candidate for the determination of *E. coli* O157:H7 in biological and clinical applications.

Conflicts of interest

The authors declare that they have no competing interest.

Acknowledgements

This work was financially supported by the National Key Research and Development Program of China (No. 2016YFD0501001).

References

1 Z. X. Zhan, H. Li, J. Liu, G. Y. Xie, F. B. Xiao, X. Wu, Z. P. Aguilar and H. Y. Xu, *Food Control*, 2020, **107**, 106806.
2 B. Pang, C. Zhao, L. Li, X. Song, K. Xu, J. Wang, Y. Liu, K. Fu, H. Bao, D. Song, X. Meng, X. Qu, Z. Zhang and J. Li, *Anal. Biochem.*, 2018, **542**, 58–62.
3 L. Zhu, Y. Zhang, P. He, Y. Zhang and Q. Wang, *J. Chromatogr. B: Anal. Technol. Biomed. Life Sci.*, 2018, **1093–1094**, 141–146.
4 T. Yamaguchi, S. Kawakami, M. Hatamoto, H. Imachi, M. Takahashi, N. Araki, T. Yamaguchi and K. Kubota, *Environ. Microbiol.*, 2015, **17**, 2532–2541.
5 J. Chen, Z. Huang, Z. Luo, Q. Yu, Y. Xu, X. Wang, Y. Li and Y. Duan, *Anal. Chem.*, 2018, **90**, 12019–12026.
6 U. Farooq, Q. L. Yang, M. W. Ullah and S. Q. Wang, *Biosens. Bioelectron.*, 2018, **118**, 204–216.
7 M. Zhong, L. Yang, H. Yang, C. Cheng, W. Deng, Y. Tan, Q. Xie and S. Yao, *Biosens. Bioelectron.*, 2019, **126**, 493–500.
8 K. McCutcheon, A. B. Bandara, Z. Zuo, J. R. Heflin and T. J. Inzana, *Biosensors*, 2019, **9**, 64.
9 P. Wu, R. Huang, G. Li, Y. He, C. Chen, W. Xiao and P. Ding, *J. Nanosci. Nanotechnol.*, 2018, **18**, 3654–3659.
10 J. Ge, Y. Zhao, C. Li and G. Jie, *Anal. Chem.*, 2019, **91**, 3546–3554.
11 Z. Tang, J. He, J. Chen, Y. Niu, Y. Zhao, Y. Zhang and C. Yu, *Biosens. Bioelectron.*, 2018, **101**, 253–259.
12 J. Miao, X. Li, Y. Li, X. Dong, G. Zhao, J. Fang, Q. Wei and W. Cao, *Anal. Chim. Acta*, 2019, **1089**, 48–55.
13 Y. Liu, B. Wang, X. Ji and Z. He, *Anal. Bioanal. Chem.*, 2018, **410**, 7591–7598.
14 S. Kumari and R. P. Singh, *Int. J. Biol. Macromol.*, 2012, **50**, 878–883.
15 X. Yu, L. Hu, H. He, F. Zhang, M. Wang, W. Wei and Z. Xia, *Anal. Chim. Acta*, 2019, **1057**, 114–122.
16 M. Negahdary and H. Heli, *Recent Pat. Nanotechnol.*, 2018, **12**, 22–33.
17 J. Cui and S. Jia, *Coord. Chem. Rev.*, 2017, **352**, 249–263.
18 R. Jin, D. Kong, X. Zhao, H. Li, X. Yan, F. Liu, P. Sun, D. Du, Y. Lin and G. Lu, *Biosens. Bioelectron.*, 2019, **141**, 111473.
19 J. Ge, J. Lei and R. N. Zare, *Nat. Nanotechnol.*, 2012, **7**, 428–432.
20 N. Akhtar, S. K. Metkar, A. Girigoswami and K. Girigoswami, *Mater. Sci. Eng., C*, 2017, **78**, 960–968.
21 K. Y. Wang, S. J. Bu, C. J. Ju, C. T. Li, Z. Y. Li, Y. Han, C. Y. Ma, C. Y. Wang, Z. Hao, W. S. Liu and J. Y. Wan, *Bioorg. Med. Chem. Lett.*, 2018, **28**, 3802–3807.
22 K. Y. Wang, S. J. Bu, C. J. Ju, Y. Han, C. Y. Ma, W. S. Liu, Z. Y. Li, C. T. Li and J. Y. Wan, *Mikrochim. Acta*, 2019, **186**, 57.
23 C. Zhou, H. Zou, M. Li, C. Sun, D. Ren and Y. Li, *Biosens. Bioelectron.*, 2018, **117**, 347–353.
24 X. L. Fan, H. Y. Li, W. Y. Ye, M. Q. Zhao, D. N. Huang, Y. Fang, B. Q. Zhou, K. F. Ren, J. Ji and G. S. Fu, *Colloids Surf., B*, 2019, **183**, 110423.
25 K. C. de Almeida, T. B. Lima, D. O. Motta, O. N. Silva, B. S. Magalhaes, S. C. Dias and O. L. Franco, *J. Antibiot.*, 2014, **67**, 681–687.
26 F. Radom, P. M. Jurek, M. P. Mazurek, J. Otlewski and F. Jelen, *Biotechnol. Adv.*, 2013, **31**, 1260–1274.
27 S. M. Taghdisi, N. M. Danesh, M. A. Nameghi, M. Ramezani, M. Alibolandi, M. Hassanzadeh-Khayat, A. S. Emrani and K. Abnous, *Biosens. Bioelectron.*, 2019, **123**, 14–18.
28 M. Majdinasab, A. Hayat and J. L. Marty, *TrAC, Trends Anal. Chem.*, 2018, **107**, 60–77.
29 V. Mazzaracchio, D. Neagu, A. Porchetta, E. Marcoccio, A. Pomponi, G. Faggioni, N. D'Amore, A. Notargiacomo, M. Pea, D. Moscone, G. Palleschi, F. Lista and F. Arduini, *Biosens. Bioelectron.*, 2019, **126**, 640–646.
30 S. J. Bu, K. Y. Wang, H. S. Bai, Y. Leng, C. J. Ju, C. Y. Wang, W. S. Liu and J. Y. Wan, *Mikrochim. Acta*, 2019, **186**, 296.
31 S. Shahrokhian and S. Ranjbar, *Analyst*, 2018, **143**, 3191–3201.
32 Z. Bagheryan, J. B. Raoof, M. Golabi, A. P. F. Turner and V. Beni, *Biosens. Bioelectron.*, 2016, **80**, 566–573.
33 L. Li, Z. Chen, S. Wang, X. Jin, L. Yang, G. Liu and J. Zhao, *Biotechnol. Biotechnol. Equip.*, 2017, **31**, 1070–1078.
34 Q. Chen, D. Wang, G. Cai, Y. Xiong, Y. Li, M. Wang, H. Huo and J. Lin, *Biosens. Bioelectron.*, 2016, **86**, 770–776.
35 S. Brosel-Oliu, R. Ferreira, N. Uria, N. Abramova, R. Gargallo, F. X. Muñoz-Pascual, A. Bratov, S. Brosel-Oliu, R. Ferreira and N. Uria, *Sens. Actuators, B*, 2018, **255**(Part 3), 2988–2995.